Computers and Electronics in Agriculture 199 (2022) 107168

Contents lists available at ScienceDirect

Computers and Electronics in Agriculture

journal homepage: www.elsevier.com/locate/compag

Ammonia emission prediction for dairy cattle housing from reaction kinetic modeling to the barn scale

Sabrina Hempel [a,*], Latifa Ouatahar [b], David Janke [a], E. Moustapha Doumbia [a], Dilya Willink [a,c], Barbara Amon [b,d], Andre Bannink [e], Thomas Amon [a,f]

[a] Leibniz Institute for Agricultural Engineering and Bioeconomy (ATB), Department Livestock Engineering, Max-Eyth-Allee 100, Potsdam 14469, Brandenburg, Germany
[b] Leibniz Institute for Agricultural Engineering and Bioeconomy (ATB), Department Technology Assessment and Substance Cycles, Max-Eyth-Allee 100, Potsdam 14469, Brandenburg, Germany
[c] Lidl Digital Trading GmbH & Co. KG, Stiftsbergstraße 1, Neckarsulm 74172, Baden-Wuerttemberg, Germany
[d] University of Zielona Gora, Faculty of Civil Engineering, Architecture and Environmental Engineering, Licealna 9/9, Zielona Gora 65-417, Lubusz, Poland
[e] Wageningen University & Research, Wageningen Livestock Research, Animal Nutrition, De Elst 1, Wageningen 6708WD, Gelderland, The Netherlands
[f] Free University of Berlin, Institute of Animal Hygiene and Environmental Health, Department of Veterinary Medicine, Robert-von-Ostertag-Str. 7-13, Berlin 14163, Berlin, Germany

ARTICLE INFO

Keywords:
Dairy cattle
Ammonia
Process modeling
2000 MSC:
0000
1111

ABSTRACT

One way to estimate ammonia emission rates from naturally ventilated housing systems is to scale-up mechanistic modeling results. However, obtaining the relevant data to set initial and boundary conditions adequately is usually very challenging and for a whole barn barely possible. This study has investigated the potential of coupling different mechanistic modeling approaches towards an overarching barn scale ammonia emission model, which might permit ammonia emission projections for naturally ventilated housing systems with minimal measurement efforts. To this end, we combined an ammonia volatilization model for shallow urine or slurry puddles with a dynamic mechanistic model of digestion and excretion of nitrogen, an empirical model to estimate urination volumes, semi-empirical models for pH and temperature dynamics of the puddles and a mechanistic air flow model. The ammonia volatilization model was integrated with a time step of one second over a period of twenty-four hours, while the relevant boundary conditions were updated on an hourly base (determined by the other mentioned submodels). Projections and uncertainties of the approach were investigated for a farm case with about ten months of on-farm measurements in a naturally ventilated dairy cattle building with scraped solid floor in Northern Germany. The results showed that the nested model was in general capable to reproduce the long-term emission trend and variability, while the short-term variability was damped compared with the emission measurements. A sensitivity study indicated that particularly a refinement of the submodules for urine puddle alkalizing, urination volume and urea concentration distributions as well as for local near-surface wind speeds have a great potential to further improve the overall model accuracy. The cleaning efficiency of the scraper has turned out to be a crucial and sensitive parameter in the modeling, which so far has been described insufficiently by measurements or modeling approaches.

1. Introduction

Emissions from agricultural production are a great concern in the context of environmental protection and climate change mitigation (Lal, 2021; Amon et al., 2021). One of the most crucial substances in this context is ammonia (NH_3), the emission of which is harmful for the nearby environment as it causes large nitrogen entries into soils, water and vegetation leading to eutrophication and acidification. The resulting modifications in the regional flora (e.g., plant coverage or algae bloom) affect the Earth's surface albedo and thus indirectly the climate systems. The potential chemical reaction products of the short living NH_3 affect the climate system and are also a threat to the health of animals and humans (Cheng et al., 2021; de Vries, 2021). In particular, NH_3 is a significant source of indirect emissions of nitrous oxide (N_2O), which is a potent greenhouse gas. Moreover, it is a source of the secondary inorganic aerosols (SIA) ammonium sulfate and ammonium nitrate which

* Corresponding author.
E-mail address: shempel@atb-potsdam.de (S. Hempel).

https://doi.org/10.1016/j.compag.2022.107168
Received 7 March 2022; Received in revised form 20 June 2022; Accepted 20 June 2022
Available online 29 June 2022

occur as particulate matter in the atmosphere.

With more than 90% the majority of NH_3 emissions in Europe is attributed to agricultural production, with a tendency to further increase (Murawska and Prus, 2021). About half of those emissions is associated with livestock husbandry. The actual emission value of a husbandry system, however, depends on many factors, such as animal factors (e.g., species, production level/ yield), housing factors (e.g., floor and cleaning system, barn openings and ventilation) and environmental factors (e.g., local air temperature, local air flow patterns).

In consequence, in particular for naturally ventilated housing systems, the detailed acquisition of emission data and the assessment of the complex emission processes require extensive resource usage for on-farm measurements which are metrological challenging but also with respect to staff and costs involved. Latest expert recommendations indicate that four barns per animal category and per floor type should be measured with high-end measurement equipment over at least six independent measurement periods of at least 24 h distributed though-out the year capturing warm, cold and transient weather conditions to obtain statistically representative (average) emission values (International VERA Secretariat, 2018). However, often different temporal sampling strategies were and are used in studies (for example two farms with three times two to three weeks (Wu et al., 2012) in warm, cold and transition season, six farms with twice three days where each of the seasons occurred on two farms (Schrade et al., 2012), one farm for six month covering summer, winter and transition season (Schmithausen et al., 2018) or one farm twice for the duration of a week (D'Urso et al., 2021)). The determination of the individual emission values is in most cases based on tracer gas methods, either using an artificial tracer or the carbon dioxide (CO_2) produced by the housed animals and stored manure. Due to the imperfect mixing of used and fresh air there is an inherent, systematic uncertainty of about 20% in the tracer balance based emission estimates depending on the lateral and vertical distribution of sampling locations and the timing of the sampling (Janke et al., 2020; Hempel et al., 2020; Doumbia et al., 2021).The characteristics of the uncertainty are not fixed but depend on the ever-changing boundary conditions (and often also on the farmer as air ventilation control is in many farms still manually depending on animal requirements).

In order to overcome those problems and to avoid expensive, overarching measurement campaigns, modeling approaches were developed over the last decades as an alternative way of NH_3 emission prediction. Those approaches include, for example, balancing approaches based on nutrition and excretion modeling, reaction-kinetics models for individual urine puddles and slurry storage tanks as well as gas dispersion modeling. All of those can mimic particular aspects of the emission process. But they rely themselves on either comprehensive measurement campaigns or the usage of default values, which limits their accuracy and transferability.

The aim of this study was to investigate the potential of coupling different mechanistic modeling approaches towards an overarching barn scale model for NH_3 emissions. Our process modeling was intended to study complex emission characteristics in livestock husbandry under practical conditions using mathematical and computational approaches. By that we wanted to contribute to a deeper understanding of the emission process and support the development of simplified monitoring systems.

The study focused on the following approaches with our modeling: (1) Defining a monitoring framework for emission values of a defined husbandry system (i.e., in particular defining feeding, floor, cleaning and management strategies) that can be applied not only in research, but also in commercial farms. (2) Simplifying measurement strategies by identifying the most essential parameters and optimize the related temporal and spatial sampling strategies. (3) Estimating parameter ranges that are representative for a particular husbandry system and permit model validation. (4) Projecting the system behavior when applying particular emission mitigation measures in that system.

The farm case used in this study was a loose-housing system for dairy cattle in a building with littered lying cubicles and regularly scraped solid floor walking aisles. The overall model performance in comparison to upscaling based on standard intermittent measurements, as well as existing gaps in the nested model, are discussed in this paper.

Hypothesis and limitations. The leading hypothesis of our study was that it is possible to scale up the NH_3 volatilization from individual urine puddles to the whole barn, while avoiding extensive, time-consuming sampling, if different modelling approaches are combined.

The main limitations of our model are associated with the overall variability of the model projections (as described in detail in the discussion section). The spatial and temporal variability of the input variables used is limited to an hourly and group-wise consideration. Animal individual feeding, digestion and urination characteristics as well as variations in near-surface wind speeds within the group areas and in puddle depths are not captured. Moreover, the contribution of non-urea nitrogen to NH_3 volatilization is not taken into account. The temporal dynamics of pH are addressed by empirical relations so far, neglecting the dynamic linking of the emission of NH_3 (and carbon dioxide) with the pH value of the puddle. In consequence, our model must be expected to provide a spatially averaged and temporally smoothed emission pattern.

2. Methods

2.1. Test site

As a test site for the evaluation of NH_3 emission modeling approaches we considered a naturally ventilated dairy cattle barn with solid floor located in North-East Germany (see e.g. Hempel et al., 2020 or Janke et al., 2020 for further details). The building has a gable height of 10.73 m and a side wall height of 4.2 m. The widely open long sidewalls are facing the main prevailing wind direction which is approximately South. The total floor area of the barn is 96.15 m times 34.2 m. The barn consists of four compartments which are separated by two walking alleys. In the considered period (01–11-2016 until 27–08-2017), two compartments accommodated on average about 120 cows each and the other two on average about 70 cows each. The solid concrete alley floors were cleared by automatic scrapers every 1.5 hours. Cows went out for milking group-wise for about 45–60 minutes three times a day. Taking into consideration all four groups this resulted in a total length of each of the three milking cycles of about 3–4 hours. Milking cycles started approximately at 06:00 a.m., 02:00 p.m. and 10:00 p.m. Feed was provided around 06:45 a.m. and 10:30 a.m. as a total mixed ration. Concentrations of CO_2 and NH_3 were monitored inside and around the barn on a hourly basis using a tubing system and two high-resolution Fourier Transform Infrared (FTIR) spectrometers (Gasmet CX4000, Gasmet Technologies Inc., Karlsruhe, Germany). Ten sampling Teflon tubes with an inner diameter of 6 mm and an orifice with a capillary trap every 8–10 m were placed 4 m to 8 m away from the walls. One of the lines was mounted below the roof in the middle of the barn. The other lines were mounted at approximately 3 m height. Out of the four sample lines outside the building the line with the lowest CO_2 value was selected to represent outdoor gas concentrations, i.e. the background concentration of the incoming air. In order to determine the concentration of the outgoing air we followed two different approaches (cf. Janke et al., 2020 for details): (1) The averaging approach. This approach involved the mean of the six sample lines inside the building to represent indoor gas concentration. By definition, it tends to systematically underestimate indoor gas concentrations, but it is rather robust with regard to random errors induced by fluctuating wind directions. (2) The wind-driven approach. In this case, the gas concentration values of up to two of the indoor sample lines were considered dependent on the wind corridor associated with the inflow conditions at the respective hour of the gas measurements. The selected lines for the individual wind corridors are summarized in Table 1. This approach is in general very sensitive to changes in the wind direction that are faster than the gas sampling

Table 1
Definition of wind corridors and associated selection of indoor gas sampling lines for the determination of the gas concentration in outgoing air.

wind corridor	considered sampling line(s)
$[0°, 25°] \cup [335°, 360°]$	north
$(25°, 65°)$	north and west
$[65°, 115°]$	west
$(115°, 155°)$	south and west
$[155°, 205°]$	south
$(205°, 245°)$	south and east
$[245°, 295°]$	east
$(295°, 335°)$	north and east

frequency, but the systematic error associated with mixing of fresh and used air is considerably smaller than in the averaging approach.

Simultaneously to the gas concentrations, air temperature was measured at a distance of 5 m from the building with an EasyLog USB 2 + sensor (Lascar Electronics Inc., Whiteparish, UK) and inflow wind velocity was obtained from an anemometer (Windmaster Pro ultrasonic anemometer, Gill Instruments Limited, Lymington, Hampshire, UK) that was mounted on the roof of the building at a height of about 12 m.

Compartment-wise animal data was provided by the barn's administration. This data included number, average animal mass, milk yield and composition, dry matter intake (DMI) and feed chemical composition.

In the case of gaps in the input data (i.e., air temperature, inflow wind speed, inflow direction, number of animals, average animal mass and average milk yield) a linear interpolation based on the preceding and subsequent value in the dataset was used. Moreover, for the comparison between measured and modeled emissions, timestamps were omitted if no gas measurements were available or the gas concentration difference between indoor and outdoor air was negative.

2.2. Physico-chemical barn scale model

Our mechanistic barn scale NH_3 emission model involves the following main elements: As a model core, differential equations describing the release of NH_3 from individual urine puddles were taken from literature (cf. Section 2.2.1). This model core required an input of the initial total ammoniacal nitrogen (TAN) and urea concentration, pH and temperature of the emitting urine puddles and near-surface wind speed as well as effective emission active surface area. Submodels were used to estimate these relevant input parameter as illustrated in the scheme in Fig. 1.

The first submodel was a pH model (cf. Section 2.2.2 for details). It determined the pH of the slurry puddle (i.e. a puddle of cattle urine mixed with feces) as a function of the initial urine pH value (either estimated based on the the dietary cation anion difference or from urine samples) and the rate of pH change over time.

The second submodel was a dynamic and mechanistic model of rumen microbial fermentation processes, representing the processes of digestion in the gastrointestinal tract (cf. Section 2.2.3 for details). This submodel was used to estimate total nitrogen excretion, fecal nitrogen digestibility and the amount of nitrogen excreted in urine (often referred to as TAN), urine volume, and the initial value of TAN concentration.

The third submodel was a volume urination model (cf. Section 2.2.4) for details). It estimated the urination volume in dependence of the time of the day, the DMI, fractions of Na and K in the diet and milk composition. Together with the output of the dynamic mechanistic model of microbial fermentation processes, this permitted an estimation of the urea concentration in the urine at different hours of the day. Moreover, it provided an estimation of the initial emission active surface area in the course of the day. The effective surface area was then updated on an hourly basis in the model core taking into account the scraping frequency and efficiency.

The forth submodel was a cooling model (cf. Section 2.2.5). It estimated the temperature of urine puddles at the emission active surface, starting from approximately body temperature of the cows and considering the exponential decrease of the temperature difference between the puddle and the ambient air.

The fifth submodel was a flow model (cf. Section 2.2.6). Simulations of a computational fluid dynamics model were used to translate inflow wind speed into average near-surface wind speed taking into account geometric boundary conditions, the dominating convection scheme and the wind's angle of attack.

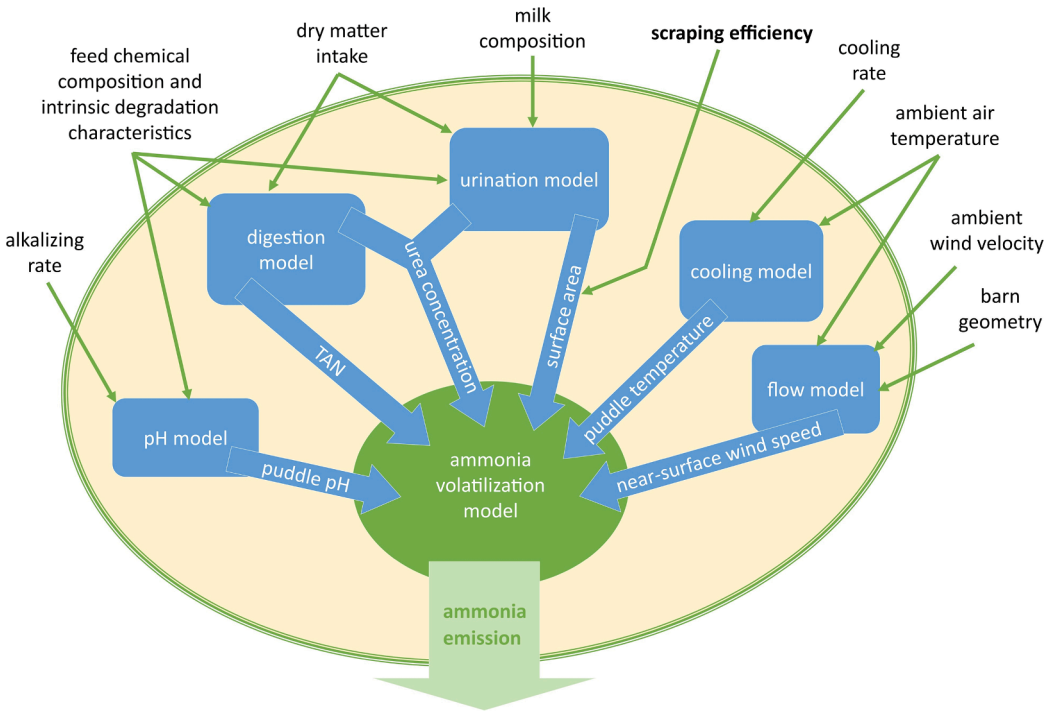

Fig. 1. Scheme of the physico-chemical barn scale NH_3 emission model with its multiple submodels and the required input parameters.

2.2.1. Ammonia volatilization model

The reaction kinetics of NH_3 volatilization from urine puddles were calculated based on differential equations given in Eq. 1 and Eq. 2 as well as the mass transfer coefficient (Eq. 3), the Henry constant (Eq. 4) and and the NH_3 fraction (Eq. 5) proposed in literature (Elzing and Monteny, 1997; Monteny et al., 1998). This model core covered enzymatic, dissociative and evaporative processes affecting the emission source strength.

$$\frac{dU_c}{dt} = -S_m \cdot U_c \cdot (K_m + U_c)^{-1} \quad (1)$$

$$\frac{dTAN_c}{dt} = -k \cdot A \cdot TAN_c \cdot f \cdot (H \cdot V)^{-1} + 2 \cdot S_m \cdot U_c \cdot (K_m + U_c)^{-1} \quad (2)$$

$$k = 48.439 \cdot (v^{0.8}) \cdot (T^{-1.4}) \quad (3)$$

$$H = 1384 \cdot (1.053^{(293-T)}) \quad (4)$$

$$f^{-1} = 1 + [10^{-pH} \cdot (0.81 \cdot 10^{-10} \cdot 1.07^{T-293})^{-1}] \quad (5)$$

The relevant variables and parameter in the equations are defined in Table 2.

We considered hourly urination events leading to NH_3 release from the barn floor. For each urination event, we performed the integration of the differential equations over a period of 24 h, with an integration step width of one second and an update of the input parameters urine puddle temperature and pH every hour. We derived the emission active surface area from the urination volume associated with the initial hour of integration following Eq. 6.

$$A = V_{urine} \cdot pd \quad (6)$$

with V_{urine} the estimated urination volume of all cows in the group in the respective hour given in $m^3\,h^{-1}\,group^{-1}$ and an assumed average puddle depth pd given in m. We assumed here that all urine remained on the floor as long as there was no scraping activity. Moreover, during the integration procedure, we assumed that the emission active surface area was reduced by a factor c at each hour with scraper activity sh. In consequence, the hourly emission of a distinct hour was calculated as sum of emissions from all urination events within the last 24 h. (See Fig. 2)

2.2.2. The pH model

The logistic regression equation (Eq. 7 that calculates the initial pH value of urine) was derived from a publication of Oenema (2008) (that was itself based on a preceding study of Bannink and Vuuren (1998)) with $R^2 = 0.692$ and SE $= 0.612$ (Bannink and van Vuuren, 1998; Oenema et al., 2008).

$$pH_{initial} = 5.72 + 2.57(1 + \exp(-0.015 \cdot \Delta_{Ion}))^{-1} \quad (7)$$

where $pH_{initial}$ is the pH of urine during an urination event and Δ_{Ion} is the dietary cation anion difference. For the estimation, we needed data on the Sodium (Na), Potassium (K), Chloride (Cl) and Sulfur (S) content in dietary dry matter (DM). The dietary cation anion difference was then calculated as (Na + K-Cl-2·S) in the unit of meq/kg feed DM. Here meq was the unit used by dividing the milligrams by the atom weight to derive moles of Na, K, Cl and S. Positive charges (Na and K) were weighted against the negative charges (Cl and S). So the gram of Na, K, Cl an S in dietary DM had to be divided by 23, 39, 35.5 and 80, respectively to obtain meq of Na, K, Cl and S. Only the S was multiplied by 2 because it is excreted in the form of SO_4, which has is a double negative charge. The higher the dietary cation anion difference, the higher the urine pH. With a decrease of this difference to values beneath + 100 meq/kg DM the urine pH starts to drop considerably.

When detailed data on the dietary cation anion difference was missing, the initial pH value in the model was set to a default value (based on measurements at the test site barn). We further assumed an alkalizing of the slurry puddle in the course of time due to the emission of CO_2 and NH_3 as described in literature (Snoek et al., 2016). The pH increase was modeled by two exponential terms. The first term describes a fast increase at the beginning associated with the emission of CO_2. The second term describes the slowing down of the alkalizing towards an asymptotic pH value, which has been associated in literature with the emission of NH_3.

$$pH_t = pH_{max} - 0.45 \cdot d \cdot \exp(-k1_{pH} \cdot t) - 0.55 \cdot d \cdot \exp(-k2_{pH} \cdot t) \quad (8)$$

where pH_t is the pH value after time t, pH_{max} is the asymptotic pH value to be reached at $t \to \infty$, $k1_{pH}$ and $k2_{pH}$ are the alkalizing rates associated with the emission of CO_2 and NH_3, and d is the maximal change of the pH value (i.e., $pH_{max} - pH_{initial}$). Based on observations in literature 45% of the maximal change were attributed to the CO_2 related term and 55% of the maximal change were attributed to the NH_3 related term (Snoek et al., 2016).

2.2.3. The dynamic mechanistic model of digestion and excretion of nitrogen

The nitrogen excreta via urine and feces was calculated using an extent dynamic and mechanistic model of rumen fermentation and intestinal digestion. The model provided outputs on organic matter (OM), C and N excreted in urine and feces as a function of diet composition and rumen intrinsic degradation characteristics. The model was expanded from Dijkstra (1992), and updated on N digestion by Bannink (2018) (Dijkstra et al., 1992; Bannink et al., 2018). In addition, Dijkstra (2018) introduced equations that represent the urine and fecal excretion and deliver quantitative data on excreta composition, including urine as well as feces (Dijkstra et al., 2018). The process-oriented model was based on a set of differential equations that describe the change in time of pools of substrate, micro-organisms and microbial end-product in the rumen and large intestine. When assuming a zero N retention in the body Eq. 9 applies.

$$N_{feed} = N_{urine} + N_{milk} + N_{faeces} \quad (9)$$

The unit of N_{feed} is gNd^{-1}. Milk nitrogen (N_{milk}) in gNd^{-1} was calculated from observed values of milk composition based on Eq. 10.

$$N_{Milk} = (MY \cdot PC/100) \cdot 1000 \cdot 6.38^{-1} \quad (10)$$

with milk yield (MY) expressed in $kg\,d^{-1}\,cow^{-1}$ and milk protein content (PC) in %, and with 6.3 g N per g milk protein.

Table 2
Overview of parameter and constants involved in the NH_3 volorization model. Units are provided in brackets.

A	=	emitting surface area (m^2)
f	=	ammonia fraction (dimensionless); a function of T and pH
k	=	mass transfer coefficient ($m \cdot s^{-1}$); a function of T and v
H	=	Henry's constant (dimensionless); a function of T
	=	equilibrium concentration ratio of NH_3 in liquid and gaseous phase
TAN_c	=	sum of ammonia and ammonium concentration ($mol \cdot m^{-3}$)
&=	TAN concentration	
	=	urine nitrogen per total nitrogen excretion
E	=	ammonia emission ($mol \cdot s^{-1}$)
V	=	volume of manure layer (m^3)
v	=	air velocity ($m \cdot s^{-1}$)
T	=	air temperature (K)
U_c	=	urea concentration ($mol \cdot m^{-3}$)
S_m	=	maximum conversion rate at high urea concentration (2.83 $mol \cdot m^{-3} \cdot s^{-1}$)
K_m	=	Michaelis constant (2000 $mol \cdot m^{-3}$)
t	=	time (s)

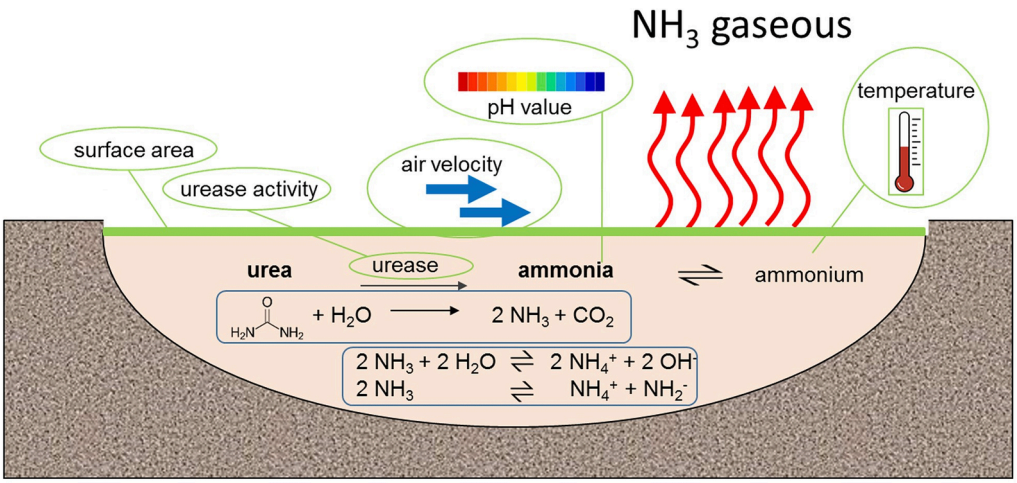

Fig. 2. Scheme of the NH_3 volatilization model with its main input parameters.

The urea concentration (U_c) in *mol* per m^3 was estimated from the nitrogen excretion in urine based on Eq. 11. Note that non-urea compounds which are art of urine nitrogen were neglected here.

$$U_c = 71.42857 \cdot N_{urine.day} \cdot (24 \cdot V_{urine})^{-1} \quad (11)$$

with $N_{urine.day}$ being the average daily amount of urine N excreted by a cow of the considered herd/group. The unit of $N_{urine.day}$ is $g N \cdot cow^{-1} day^{-1}$. The factor 24^{-1} is a conversion factor to hourly values assuming that the N excretion is uniformly distributed over all hours of the day. The factor 71.42857 is a conversion factor from g N per liter towards *mol* N per m^3, with $1\,m^3 = 1000\,l$ and a molar mass of nitrogen of $14\,g\,mol^{-1}$. We estimated the daily average urination volume from the feed intake and distributed it over the hours of the day using the urination submodel described in subSection 2.2.4. Moreover, the estimated nitrogen excretion via urine and feces permitted to approximate the TAN concentration (further denoted TAN_c) assuming that the amount of total nitrogen excreted by urination is a good approximation of TAN. The TAN concentration in the urine puddle was derived from the fraction of urine N in the total N excreted multiplied with the density of the fluid in the puddle following Eq. 12.

$$TAN_c = N_{tot.day}^{-1} \cdot N_{urine.day} \cdot \rho M^{-1} \quad (12)$$

with $N_{tot.day}$ the average total amount of excreted nitrogen per cow and day in $g N \cdot cow^{-1}$ day^{-1} and $N_{urine.day}$ the average amount of total nitrogen excreted by urination per cow and day in $g N \cdot cow^{-1} day^{-1}$. The factor $\rho \cdot M^{-1} = 71428.57 mol\ m^{-3}$ is a conversion factor from g urine N day^{-1} per g total excreted N day^{-1} towards mol N per m^3 urine puddle, with $M = 14\,g\,mol^{-1}$ molar mass of nitrogen and the slurry density assumed to be approximately that of water (i.e., $\rho \approx 1000000\,g\,m^{-3}$).

The assumption for the slurry density is a simplification, which we made here based on two pieces of information in the literature. First, manure density based on values for fresh feces and urine from dairy cattle are listed with 990 ± 63 kg/m^3 in ASAE Standards 2003 (http://large.stanford.edu/publications/power/references/docs/ASAESstandard.pdf, last access 2022–04-13). Second, it was shown in literature that the density of manure increases approximately linearly with the total solids content, where a content of about 3% total solids is associated with a density of 1000 kg/m^3 (Wang et al., 2019). The puddles on the walking alleys of the investigated cattle barn were containing mainly urine and feces, but might be mixed with small amounts of bedding material from the cubicles. Hence, a low content of total solids could be expected.

2.2.4. The urination model

The average daily urination volume was predicted from DMI, dietary content of Potassium (K), Sodium (Na), and N, milk production, and milk protein content, using an empirical equation derived from Bannink (1999) (see Eq. 13) (Bannink et al., 1999).

$$V_{urine.day} = 1.3441 + (0.001 \cdot DMI) \cdot F_{cont} - Milk \cdot Milk_{cont} \quad (13)$$

with *DMI* the dry matter intake in $g\,day^{-1}$. Milk is the uncorrected milk production in $kg\,day^{-1}$, F_{cont} is the feed composition which is defined here as the weighted sum of Na, K and N fractions in feed in gram per kilogram of dry matter (DM) (see Eq. 14), and $Milk_{cont}$ is a weighting factor that depends on the milk protein proportion (see Eq. 15).

$$F_{cont} = (0.1079 \cdot frNa + 0.0538 \cdot frK + 0.01266 \cdot fN) \quad (14)$$

with *frNa*, *frK* and *frN* being the sodium, potassium and nitrogen fractions in g per kg DM. When detailed data on Na and K was missing the default values are used, where default of *frNa* is 2.5 g Na per kg DM, and of *frK* it is 30 g K per kg DM.

$$Milk_{cont} = (0.1216 + 0.0275 \cdot frprot \cdot 100) \quad (15)$$

where *frprot* stands for the fraction of protein in milk. When data was missing a default value of 0.033 (i.e. 3.3%) is used. In order to model hourly urination the total daily urination volume was distributed over all hours of the day approximating the right-skewed distribution of urination volume per urination event reported in literature for grazing cattle (Betteridge et al., 2013; Misselbrook et al., 2016). In this context, we considered the individual urination events to be equally distributed over the day (Robichaud et al., 2011). Moreover, the model took into account an observation reported in literature that maximal volume per event was typically observed in the early morning hours (0–4 h), while minimal urination volumes were found in the last evening (20–24 h)) (Misselbrook et al., 2016). Hence, our urination submodel output involved 24 urination events, the volume of which followed the distribution shown in the upper panel of Fig. 3, where we allocated the largest event volume to 2 a.m. and then gradually decrease the volume over the day until 1 a.m. as shown in the lower panel of Fig. 3.

For hours where cows were partly absent due to milking activities, the estimated urination volume was reduced by a factor which equals the percentage of the hour that cows were suspected to be outside the barn (e.g., 0.75 if cows are out for 45 min).

2.2.5. The cooling model

The slurry puddle temperature was supposed to have initially body temperature, where we considered a sinusoidal cycle of body tempera-

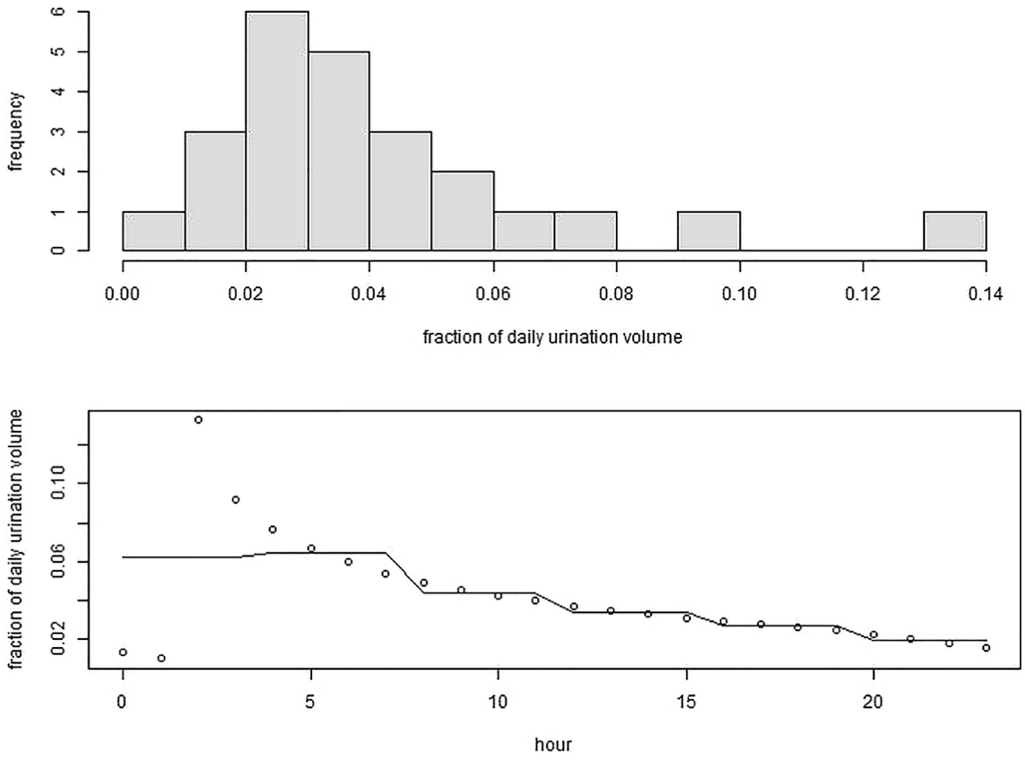

Fig. 3. The upper panel shows the distribution of urination volume per event derived based on literature data from grazing cattle and the lower panel shows the associated distribution of urination volume per time interval. The solid line is average from 0–4, 4–8, 8–12, 12–16, 16–20 and 20–0, which corresponds to the measurement intervals in the literature.

ture with minimum at 6 a.m., maximum at 6 p.m. and an average value of 38°C (Piccione et al., 2003). The emission, which resulted from one urination event, was modeled considering 24 h of integration in the model core, over which the slurry temperature was gradually decreased towards air temperature. The air temperature close to the emission active surface was estimated from the outdoor air temperature using the transfer function in Eq. 15

$$T_{air} = a_1 + a_2 \cdot T_{air.out} \tag{16}$$

where the parameter a_1 and a_2 were obtained barn-specifically from regression based on sample measurements. In the cooling submodel, we considered the comparably small volume of slurry as a body within a thermal energy reservoir represented by the air volume inside the barn. The cooling process thus could be described using the Newtonian law of cooling (see Eq. 17).

$$T_{slurry}(i) = T_{air}(i) + (T_{slurry}(i-1) - T_{air}(i)) \cdot exp(-k_T \cdot t) \tag{17}$$

Here, $T_{slurry}(i)$ and $T_{air}(i)$ are the slurry temperature and the air temperature for the next integration period in the core model, $T_{slurry}(i-1)$ is the slurry temperature in the previous period of integration, t is the time one period of integration lasts (in general we used 60 min here) and k_T is the cooling rate. The target air temperature $T_{air}(i)$ within the barn changed during the integration due to the typical daily cycle of outdoor air temperature. In the modelling, we updated the target air temperature hourly during the integration using always the air temperature of the respective hour of the day, when the integration was initialized, as an approximation. In that way the model needed only the air temperature data from one measurement day as input. The cooling rate is a model parameter which needs to be determined for each barn system to be modeled.

2.2.6. The flow model

In order to translate the inflow wind conditions to the local wind speed over the emission active surface we used the results of a computational fluid dynamics (CFD) model with four animal occupied zones modeled as anisotropic porous media (Doumbia et al., 2021). The length-to-width-ratio of the model building was two, which is a little less than the ratio for the actual test site which is about 2.8 (cf. Fig. 4(a)). As a further simplification, the geometry of the model building was fully symmetric and all animal occupied zones were of equal size so that a reduced set of incident inflow angles could be considered (e.g., the pattern for wind with 315° incident angle could be obtained from a simulation with 45° incident angle by performing a reflection with respect to the axis of symmetry, which was basically a renaming of the groups, see Fig. 4(b) for an illustration of this example).

We simulated the flow for the incident wind angles 0°, 45° and 90° as well as for three combinations of ambient temperature and inflow velocity which represented the possible convection regimes associated with typical indoor air flow patterns. The CFD simulations were based on the Reynolds-averaged Navier–Stokes (RANS) equations, i.e. a set of time-averaged equations of motion for the air flow. The turbulence properties were modeled using a k-omega turbulence model, which is a standard approach that adds two more transport equations to the RANS model in order to represent the turbulent properties of the flow which are not captured in the time-averaged equations. Further details on the CFD model can be found in Doumbia (2021) (Doumbia et al., 2021).

With the mentioned CFD model the flow right above the floor could be captured. For each of the nine simulation cases, the average wind speed in each of the four animal occupied zones 5 cm above the floor relative to the inflow wind speed was extracted as a scaling factor. The height of 5 cm was determined by the resolution of the air flow model. This level was the lowest in the model except for the floor-air-boundary where the air velocity was per definition equal to zero. The measured ambient conditions were assigned to one of the nine simulation cases and the near-surface wind speed was then determined group-wise by multiplying the actual measured inflow wind speed with the respective

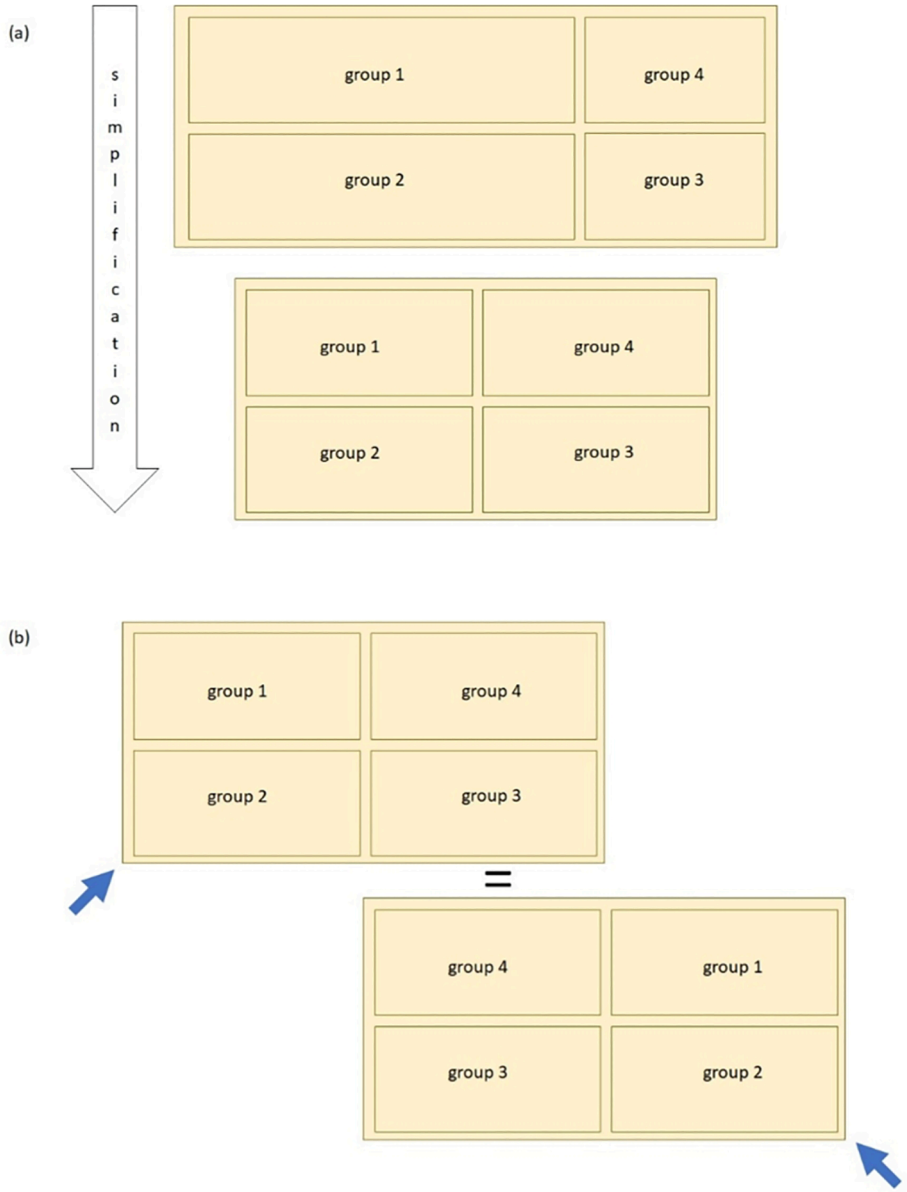

Fig. 4. The subfigure (a) illustrates the simplification from the real barn's floor plan, with length-to-width-ratio 2.8 and unequal group size towards a symmetric floor plan with length-to-width-ratio 2 and equal group sizes. The subfigure (b) illustrates how the symmetry is used to translate different inflow angles (here 315° in the upper case) into one of the simulated cases (here 45° in the lower case).

correction factor for the group under the given ambient conditions in order to account for the spatial variability of the air flow.

Moreover, based on simulations of Doumbia (2021) with the same CFD model, we derived potential retrieval factors for each of the nine simulation cases (Doumbia et al., 2021). These factors reflected the simulated deviation between the actual ratio of emitted NH_3 and CO_2 and the ratio measured at the height of 3 m given different flow patterns. The factors were 0.48 (forced convection), 0.38 (mixed convection) and 0.55 (natural convection) for cross-flow conditions, 0.62 (forced convection), 0.65 (mixed convection) and 0.84 (natural convection) for inflow via one of the gable walls, and 0.71 (forced convection), 0.68 (mixed convection) and 0.69 (natural convection) for diagonal inflow. This was an attempt to take into consideration the measurement uncertainty when validating the NH_3 emission values simulated with our mechanistic barn scale NH_3 emission model against emission values derived from CO_2 balancing.

2.2.7. *Model parameter setting*

Emissions were estimated for the four performance groups in the barn separately, since the initial and boundary conditions for the four groups differed substantially (in particular with regard to the nitrogen excretion and air flow induced shifts in chemical balances). Subsequently, the overall emission at each time step was provided as a weighted sum using the average number of cows per performance group over the simulation period as weighting factors. This way, the complex, nonlinear interaction of enzymatic, dissociative and evaporative processes and there dependency on the various input parameters could be reflected in more detail. The input parameters of the nested reaction kinetics barn scale model can be subdivided into four classes.

The first class involved **herd management data**. This involved data on DMI, feed chemical composition as well as on milk yield and composition, all of which were obtained from the farm management records. For this class the submodels were driven on inputs related to nutrition, including daily DMI, the chemical composition of the diet, and intrinsic degradation characteristics of the starch, crude protein and cell

wall material (neutral detergent fibre/ structural carbohydrates). Besides, the model also required input on dietary content of sugars, crude fat, organic acids, ash and NH_3.

The second class included **weather data** monitored in the vicinity of the barn. Those were used as input to estimate the ambient conditions near the emission active surfaces. This class involved the ambient air temperature T_{air} which was measured in 5 m distance from the barn as well as the inflow wind velocity $\vec{V}$ measured at the building's roof at a height of 12 m.

The third class grouped **estimated parameters**, which were derived based on very few sample observations, and were given a fixed value. This class included the hours of scraping activity *sh*, the average puddle depth *pd*, parameters of the transfer function from outdoor air temperature to near-surface air temperature as well as for cooling and alkalizing rates, and the initial and asymptotic pH values of the slurry puddles.

The scraping activity *sh* was estimated based on the scraping frequency in the observation period, where cleaning was performed every 90 min. The initialization hour of the scraper was assumed to be around 2 pm based on sample observations of scraping activity within the observation period. This was, however, not constantly monitored and in reality may have varied over the observation period as the scraper was turned on at arbitrary time points after any failure or maintenance.

The average puddle depth *pd* was assumed to be around 2 mm (no measurements available, the assumption is based on observations of Snoek (2016) at different dairy cattle farms with concrete floor (Snoek et al., 2016)).

The parameter a_1 and a_2 for the transfer function from outdoor air temperature to near-surface air temperature were obtained from regression over 3 h of measurements as $a_1 = 0.8369$ and $a_2 = 0.9446$.

The parameter k_T denotes the cooling rate of urine in contact with floor and ambient air. For the test case samples collected at 12 randomly distributed location at the floor of the test site in December 2018 were considered. At each sampling location air temperature and slurry temperature at the time of sample collection was monitored. For the estimation of the average cooling rate we assumed that the age of the slurry was between one minute and one hour. For each possible age a slurry temperature was estimated using Eq. 17 where k_T was varied between 0.01 and 0.05. For each of the twelve samples the combination of cooling rate and age that resulted in the smallest deviation from the measured slurry temperature was selected. The final k_T for the simulation was then considered as the average over the estimated cooling rates for the twelve samples.

For the initial pH value of urine we considered the lowest value observed in floor measurement during the measurement campaign in December 2018 at the test site barn, namely a pH value of 6.8. It has to be noted that the age of the individual measured urine or slurry puddles was unknown and the measured pH values differed considerably from each other with a mean of 7.68 and standard deviation of 0.52. Thus, the assumed initial pH value here was a rather arbitrary choice for a proof of concept.$k1_{pH}$ and $k2_{pH}$ are alkalizing rates of urine in contact with floor and ambient air. We estimated these values using the same set of samples as for the cooling rate and the estimated age of the samples. A range of 0.5 to 7 and 0.1 to 2 was tested for $k1_{pH}$ and $k2_{pH}$, respectively. The parameter combination which resulted, averaged over all twelve samples, in the smallest deviation between measured and modeled pH was taken for the simulations.

The value of the asymptotic pH value pH_{max} was estimated based on the observations of Snoek (2016), who found at different farms that after 4 h pH of slurry did not considerably increase anymore and the increase of pH between the first 4 h had on average a slope of 0.15. Hence, we took as asymptotic value the largest observed pH value (which was assumed to correspond to the oldest measured puddle) plus 0.15·4.

Finally, the forth class involved the remaining **tuning parameters**, which eventually included only one parameter, namely the cleaning efficiency *c*. This parameter describes the remaining proportion of effective emission active surface area after scraping. A range between 0.2 and 0.8 was considered for the model tuning as no measurements were available. For the tuning of the model, we used the correlation with and relative deviation from the CO_2 balance based estimation of emissions for five measurement days to select a suitable value of *c*. We repeated the procedure with five different five day periods associated with different seasons. From each five day period of input data we obtained modeled emissions over six days. The first and the last day were, however, excluded from the calculation of correlations and relative deviations as not the full set of inputs was available in those periods.

3. Results

3.1. Model tuning

Since the remaining proportion of effective emission active surface area after scraping could not be derived from the available measurements we performed the sensitivity study described in Section 2.2.7 to identify suitable values of the parameter *c*. The five selected periods involved average air temperatures of 1.5 °C, 3.8 °C, 7.4 °C, 11.4 °C and 19.0 °C. Average inflow wind speeds were around 0.8 m s^{-1}, except for one period with an average inflow wind speed of 1.3 m s^{-1}. First, we investigated the correlations between the simulated emissions and the emissions derived from gas measurements with the two different approaches to derive the indoor air concentrations as described in Section 2.1 (see Fig. 5 upper panels). The correlation was found to vary considerably depending on the considered period and the approach used to estimate the indoor concentrations from the gas concentration measurements. In several cases, we observed even a pronounced anti-correlation. The correlation was slightly improved when taking into account the suspected retrieval factor, but there was no clear trend. Moreover, it can be seen in Fig. 5 that in most cases the correlations were higher for lower values of *c*. The variations among the different cases were, however, much larger than the variation dependent on the value of *c*.

Nevertheless, the *c* value had a strong influence on the projected average emission value and the average relative deviation from the measurements, as can be seen in the middle and lower panels of Fig. 5. Lowest relative deviations were typically observed for *c* values slightly above 0.4, where the derived optimum of *c* was 0.01 to 0.02 higher if the suspected retrieval factor was taken into account. For higher ambient air temperatures and higher wind speeds the *c* value tended to be slightly lower. But as this trend was not very pronounced for the further analysis a constant value of *c* was assumed. Moreover, as the value of the retrieval factor was associated with a high level of uncertainty, while there was no clear trend for improvement of the projection, a focus was laid on the unscaled model projections for the further analysis. For the subsequent simulations we considered two cases, namely $c = 0.41$ and $c = 0.42$, which were associated with reasonable values of *c* according to the pre-analysis in Fig. 5.

3.2. Long-term simulation

We simulated the NH_3 emission dynamics of the test site over a period of 302 days using the input parameter settings described in the methods section and with the values $c = 0.41$ and $c = 0.42$ (cf. Section 3.1). The resulting time series of hourly emission values are shown in Fig. 6 in comparison with the two versions of the CO_2 balancing to derive indoor air concentrations. We observed that the general long-term trend was well reproduced by the simulations, with correlation of emissions estimated using the averaged indoor gas concentrations ($\rho_{avg} = 0.62$) being much better than the correlation of emissions estimated using the wind-dependent selection of sampling lines ($\rho_{wind} = 0.35$). It is noted here that the two measurement-based emission time

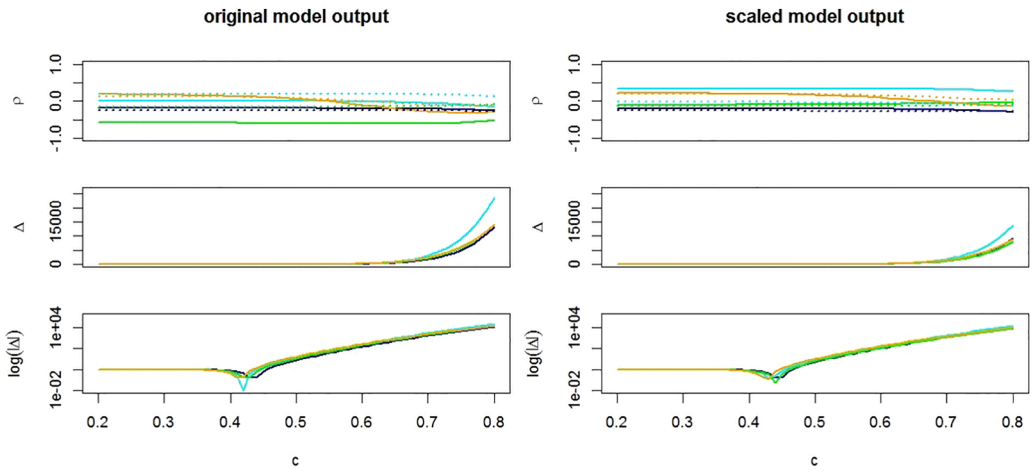

Fig. 5. Emission projection with the full model using input data for five times five days and varying the cleaning efficiency parameter c from 0.2 to 0.8. The upper panel shows the variation in resulting Pearson correlation ρ between the model projection and the estimation based on different CO_2 balancing approaches (solid lines = with averaged indoor concentration, dashed lines = with wind dependent indoor sample lines). The middle panel shows the relative deviation Δ between the model projection and the estimation based on CO_2 balancing using the average indoor concentrations. The lower panel is analog to the middle panel, but showing the absolute value of the relative deviation on a log scale. The left panels were calculated based on the actual model projections, while for the right panels the model projections were scaled with a retrieval factor derived from CFD simulations. This factor depended on the suspected convection regime and inflow wind angle (see Section 2.2.6). In all cases the different colors indicate the five differen.t trial periods.

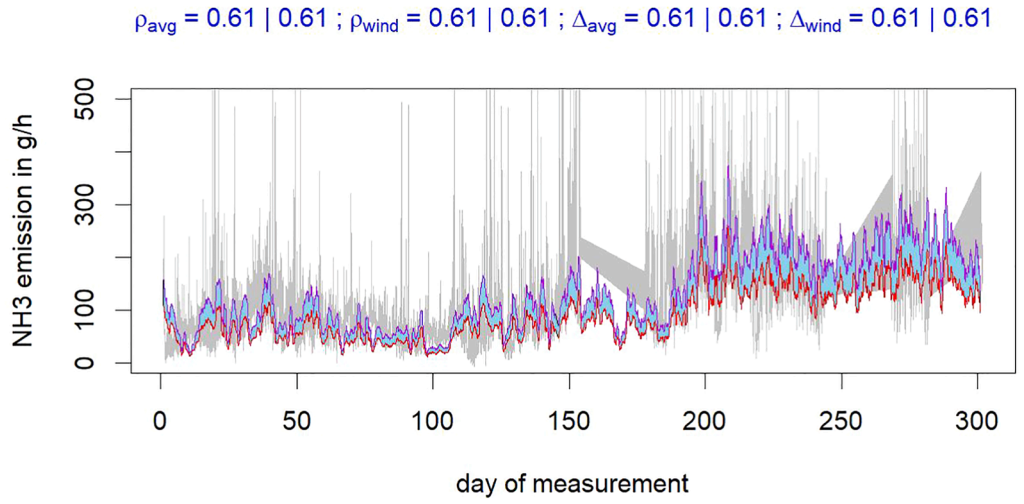

Fig. 6. Emission estimation based on CO_2 balancing versus emission projection with the barn scale model. The gray area indicates the range of emission values derived from the two approaches for the CO_2 balancing (i.e. averaged indoor concentration versus wind-dependent selection of indoor sample lines). For periods without balancing data the values are linearly interpolated. The purple curve represents the emission projection using the value $c = 0.42$, while the red curve is associated with the simulation using the value $c = 0.41$. The blue area indicates the deviation between the two simulation runs. In addition, for the two simulation cases the correlation (ρ) with and the average relative deviation (Δ) from the emission values based on the two CO_2 balancing approaches is shown. The first values always corresponds to the simulations with $c = 0.41$ and the second values to the simulations with $c = 0.42$. The indices "avg" and "wind" refer to the two balancing approaches to compare with.

series, which resulted from the two approaches of CO_2 balancing, showed a correlation of $\rho_{bal} = 0.48$, which is right in the middle of the before mentioned correlations of these two with the simulated emission data. Moreover, the average emission values, that were derived from the two measurement-based emission time series, differed by approximately 27 g per hour.

Since the estimations based on the wind-dependent selection of sampling lines were in general larger than those based on the averaged indoor concentrations, the relative deviation of the simulations from the balancing results were lower in the case of the wind-dependent selection (while the absolute value of the relative deviation could be also higher as in the simulation with $c = 0.41$). The range of the average relative deviations over all of the four combinations was close to the range of uncertainty of the measurements which is assumed to be around $\pm 20\%$ in literature (i.e., ± 0.2 relative deviation between the supposed true value and the measured value).

Moreover, Fig. 6 indicates that the projected emission dynamics showed much less fluctuations than the measurements. In consequence, the relative deviations per time point (shown in Fig. 7) were much higher than the average relative deviation. While the largest absolute deviations were predominantly negative (i.e. emission values obtained by CO_2 balancing were much higher than the simulated emission values), the largest relative deviations were in general positive (i.e., here the model overestimated the emission value). This indicated that overestimation can be observed rather in situations where the balancing based emission values are small.

At the same time, we found that the relative deviations per time point were less extreme when the wind-dependent CO_2 balancing approach was used for the evaluation, even though the correlation between balancing and simulation results was worse in this setting. In Fig. 8 we further investigated the boundary conditions under which larger relative deviations between the model and the balance based emission estimations occured. Here it was clearly visible that the very large relative deviations (i.e., much more than 100% in absolute values) were associated with situations where the measured gas concentration differences were particularly small. This means that the very large deviations were observed for times points where the uncertainty in the CO_2 balancing approaches was particularly high. At the same time about half of the

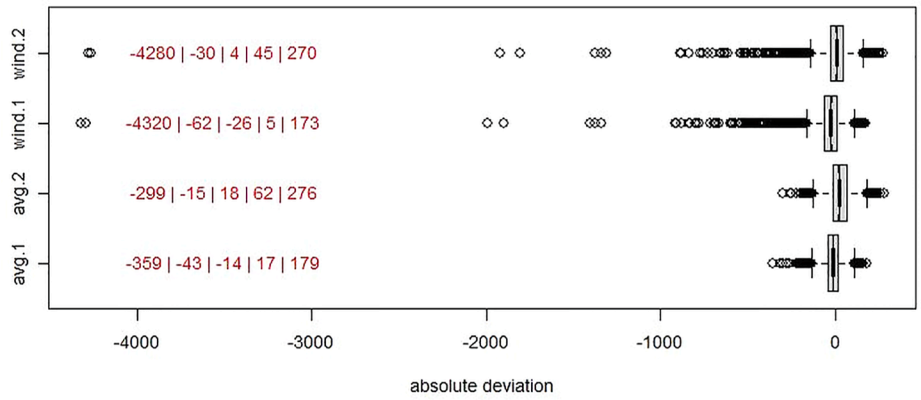

Fig. 7. Distribution of the absolute deviations (in gramm of NH_3 per hour) and relative deviations per time point for the two simulation runs (index "1" for $c = 0.41$ and index "2" for $c = 0.42$) in relation to the estimations based on the two CO_2 balancing approaches (index "avg" for the averaged indoor gas concentration and index "wind" for the wind-dependent selection of the indoor sampling lines). Negative values indicate an underestimation by the simulation compared to the experimentally derived emission values. The blue lines in the bottom panel indicate the region of less than ± 1, i.e. 100% deviation. The red numbers indicate the respective quantiles (i.e., minimum | 25% | median | 75% | maximum) for the different cases.

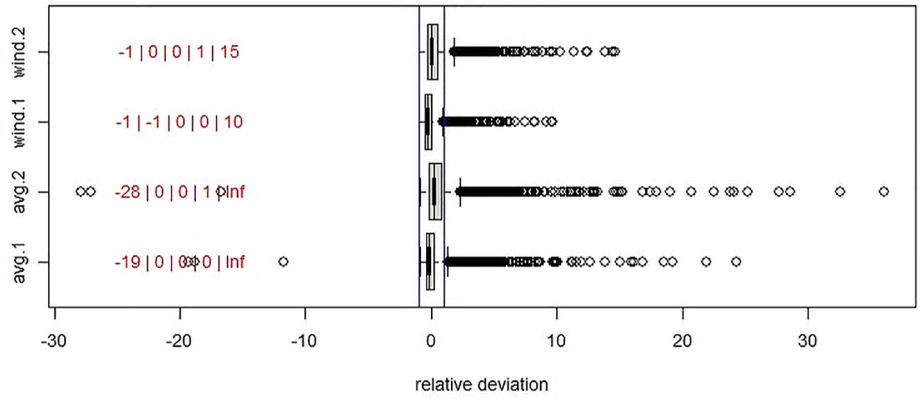

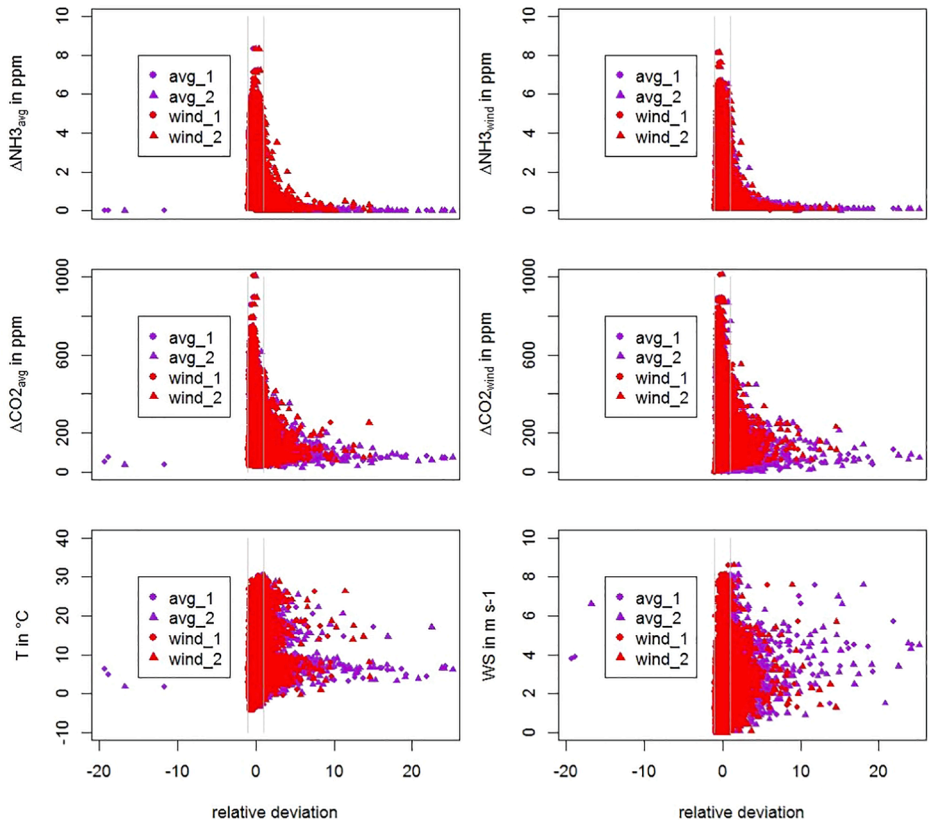

Fig. 8. Spread of measured boundary conditions in dependence on the relative deviations per time point for the two simulation runs (index "1" for $c = 0.41$ indicated by circles and index "2" for $c = 0.42$ indicated by triangles) relative to the estimations based on the two CO_2 balancing approaches (index "avg" for the averaged indoor gas concentration indicated by red color and index "wind" for the wind-dependent selection of the indoor sampling lines indicated by purple color). The upper row show the relation between the derived difference between outdoor and indoor NH_3 concentration for the two CO_2 balancing cases. The middle row displays the relation similarly for the derived differences between outdoor and indoor CO_2 concentration. Finally, the bottom row shows the relation to the measured ambient air temperature and the measured inflow wind speed. In all subpanels the grey vertical lines indicate $\pm 100\%$ relative deviation.

measured concentration differences were in this rather low concentration range as can been seen in Fig. 9.

For the relation between the wind speed and the relative deviations between model simulations and CO_2 balances we found no clear pattern in Fig. 8. Only for very high and very low wind speeds the observed relative deviations were in general less extreme. While these very high wind speeds were very rare in the dataset, the very low wind speeds were associated with about one third of the cases as indicated by the normalized cumulative frequency distribution in Fig. 9.

Finally, we observed occurrence of higher differences between the model simulations and the CO_2 balancing results for distinct temperature ranges, namely around 5°C, around 15°C and around 25°C (cf. Fig. 8). Nearly half of the observed temperature values were in the range between 0°C and 10°C and about one third in the range between 10°C and 20°C, where around 10°C comparatively few data were present in the dataset.

3.3. Sensitivity study

In order to investigate the sensitivity of the simulation on the individual submodels we sequentially turned off individual submodels which were replaced by simplified parameters for the core model. All results were compared among each other and with the CO_2 balancing based on the averaged indoor concentration.

In the case of the pH we compared the option "dependent" (i.e., with the alkalizing process as described in the methods section) with the option "asymptotic" (i.e., the pH is set to the maximal value already in the first integration step), the option "average" (i.e., the pH is fixed at the average value between initial and maximal value) and the option "initial" (i.e., the pH is fixed at the initial value). As shown in Fig. 10 upper panel, the higher pH values resulted in general in higher emission values and in a better alignment with the measured emissions. Keeping the pH at the initial value or at the mean of initial and asymptotic pH value all the time resulted in an average emission value almost two orders of magnitude lower than in the CO_2 balancing result. For very high pH values the average emission value was met quite well, but the correlation went down drastically as the simulated emission stayed low even for high ambient temperatures (cf. Fig. 10 and Table 3). Only the case with the changing pH value was capable to reproduce the long-term trend in the emission pattern (particularly the differences between summer and winter). This highlights that the interaction between pH and temperature in the model plays a key role in the modeling of the emission dynamics. At the same time, as shown in Table 3, setting the pH value already to the asymptotic value in the beginning of the integration resulted in a strong decrease of the correlation, while the other two tested options affected the correlation only marginally.

The lower panel of Fig. 10 shows the sensitivity study of the slurry temperature modeling. We compared four options with each other, the "cooling", "ambient", "daymean" and "average" options. The "cooling" option refers to the full model described in the methods section. In the ambient option, the slurry temperature was set to ambient temperature already in the first integration step. With the "daymean" option the slurry temperature was set equal to the ambient daily mean temperature associated with the excretion event in all integration steps. Finally, the "average" option refers to the slurry temperature fixed at the average value between body and ambient air temperature. It was noted that the options "cooling", "ambient" and "daytime" resulted in very similar emission patterns, which is also reflected in the corresponding correlation coefficients in Table 3. In the option "average", where the slurry temperature was kept constantly at (most of the time) unrealistic values, the simulated emission pattern was considerably different. Particularly, in periods with rather cold ambient conditions (i.e., first ca. 100 days), where the assumed temperature in this approach was most of the time too high, the emissions were considerably overestimated. On the other hand, in periods with rather warm ambient conditions (i.e., last ca. 100 days), where the averaging approach implies that at the beginning of the emission process the assumed temperature was too low, the emissions were underestimated. This temperature dependent bias was also reflected in the considerable anti-correlation indicated by the correlation coefficients for the option "average" in Table 3.

Next, we investigated the effect of the downscaling approach for the ambient wind speed on the overall model performance. In Fig. 11, we compared the option "CFDgroups" (i.e., simulated emissions based on the full model) with the options "CFDaverage" (i.e., one scaling factor averaged over the four groups to downscale the ambient wind speed), "logprofile" (i.e., downscaling assuming a logarithmic wind profile) and "inflow" (i.e., no downscaling). All options were in general capable to reproduce the long-term dynamics of the emissions (i.e., higher values in summer, lower in winter). The option "inflow" resulted in general in the largest emission peaks, while "logprofile" and "CFDaverage" represented more smoothed patterns. The correlation coefficients in Table 3 highlighted that the downscaling approaches that were not spatially resolved, could improve the matching between simulated and experimentally derived emissions only marginally. In contrast, the group-specific downscaling of the wind speed increased the correlation considerably from 0.51 to 0.62.

Finally, we investigated the effect of the urination distribution and found that the diurnal rhythm of the excreted urination volume can have a considerable influence on the emission dynamics. The lower panel of Fig. 11 shows the urination sensitivity study. The options "grazing" (i.e., from the full model), "exponential", "uniform" and "triggered" were compared. The "exponential" option refers to an exponential decay of urination volume from morning to night, which can be considered as a smoothed version of the "grazing" case pattern. The "uniform" points to an uniform distribution of the total urine volume over the day, which reflects observations on Holstein cows in a freestall barn showing a more

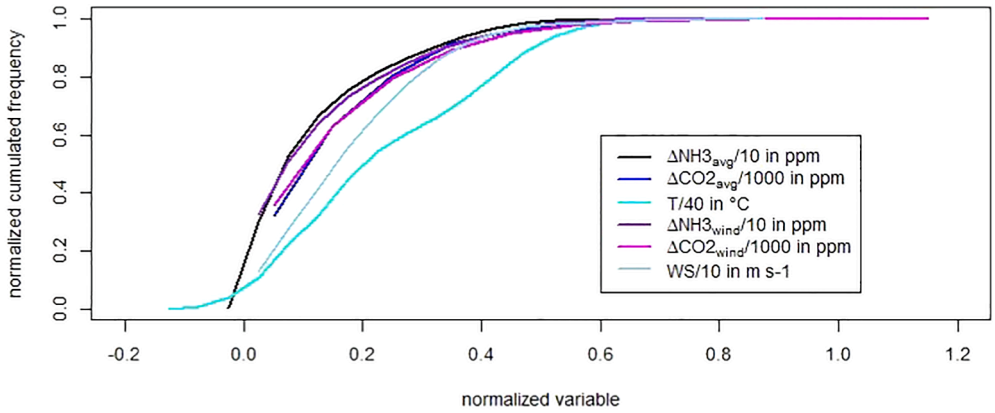

Fig. 9. Normalized cumulative frequency distribution of the measured boundary conditions shown in Fig. 8. Here, $\Delta NH3_{avg}$ and $\Delta CO2_{avg}$ are the concentration differences of NH_3 and CO_2 as estimated using the averaging approach in the CO_2 balancing as described in Section 2.1. Similarly, $\Delta NH3_{wind}$ and $\Delta CO2_{wind}$ are the concentration differences of NH_3 and CO_2 as estimated using the wind-driven approach. Moreover, T refers to the air temperature measured near the building and WS refers to the speed of the approaching wind as measured at the top of the roof of the building. The scaling factors 10, 40 and 1000 have been selected to map all of the mentioned variables to a comp.arable codomain.

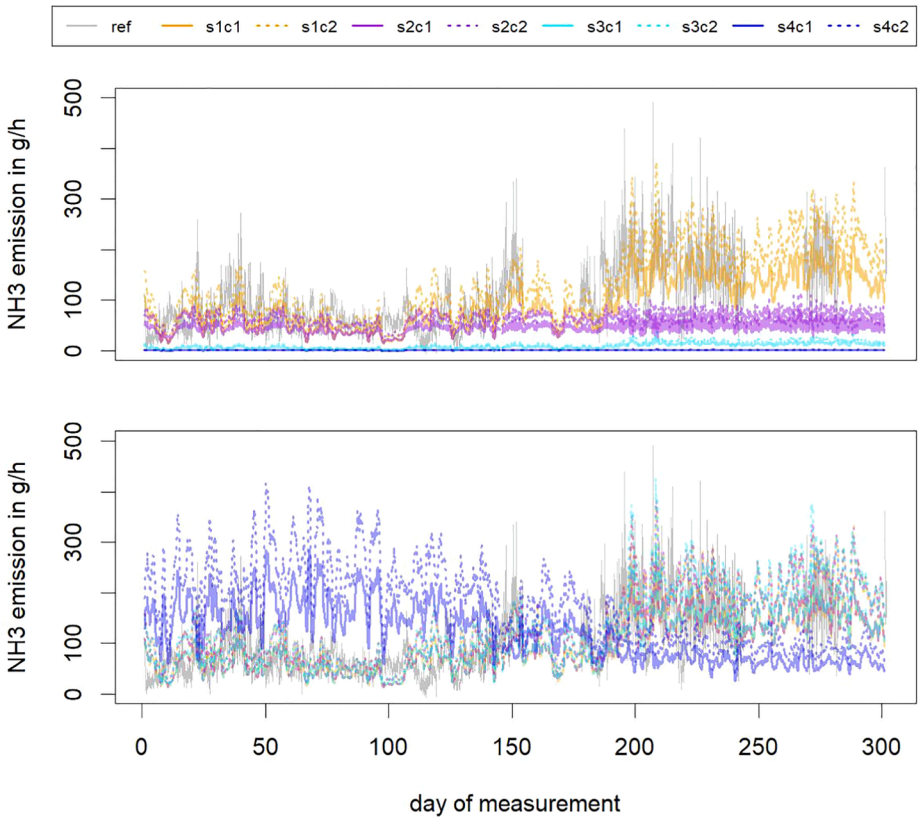

Fig. 10. Sensitivity of the simulated emission dynamics to different pH and slurry temperature models. Comparison between the CO_2 balance based emission estimation using averaged indoor gas concentrations (denoted "ref") and different simulation cases where $c1 = 0.41$ and $c2 = 0.42$ refer to the assumed value of scrapping efficiency. The full model includes the alkalizing of the slurry as a consequence of the emission processes, the cooling of the urine puddles from body to ambient temperature in the course of time, the downscaling of the wind speed from inflow reference to group specific near-surface wind speed and excretion behavior documented in literature for grazing cattle. In the case of the pH sensitivity study in the upper panel, we compared the option "s1:dependent" (i.e., from the full model) with the options "s2:asymptotic" (i.e., the pH is set to the maximal value already in the first integration step), "s3:average" (i.e., the pH is fixed at the average value between initial and maximal value) and "s4:initial" (i.e., the pH is fixed at the initial value). In the T sensitivity study in the lower panel, we compared the option "s1:cooling" (i.e., from the full model) with the options "s2: ambient" (i.e., slurry temperature is set to ambient temperature already in the first integration step), "s3:daymean" (i.e., slurry temperature is set equal to the ambient daily mean temperature associate with the excretion event) and "s4:average" (i.e., slurry temperature is fixed at the average value between body and ambient air temperature).

uniform pattern of urination over the day (Robichaud et al., 2011). The "triggered" option concerns an almost uniform distribution of the total urine volume over the day where hours with feeding or milking activity were double-weight as literature suggests that urination is more likely in active phases than during resting periods (Aland et al., 2002; Robichaud et al., 2011). It can be seen that the "grazing" and "exponential decay" distributions resulted in higher emission values than the "uniform" and the "triggered" options. A urination distribution with exponential decay from morning to night (as a simplification of the full model) had only marginal effects on the correlation and the average emission values (cf. Fig. 11 lower panel and Table 3, the average emission value differed by about 1 g per hour among the simulated options). In contrast, distributing the daily urination volume equally over the hours of the day actually improved the correlation with the balancing based emission estimation from 0.62 to 0.64. At the same time, the projected average emission value increased by about 5 g per hour. A distribution of the total urination volume where the hours of the day with feeding and milking activities were weighted twice compared to other hours, resulted in comparable correlation values. The average emissions were about 1 g per hour lower (probably because a larger portion of the urination happened outside the barn during milking under this assumption).

4. Discussion

4.1. General model performance

The presented barn scale NH_3 emission model including its submodules for animal excreta, pH, temperature and air flow, was in general capable to reproduce the long-term emission patterns based on input variables that can be easy and cost efficiently measured. With −33% to 25% (depending on the selected value for the cleaning efficiency and the selected baseline experimental reference, namely the averaging or the wind-driven approach for CO_2 balancing) the deviations between the modeled and the measured long-term average emission value were in the same order of magnitude as the deviation between the emission values obtained by the two CO_2 balancing approaches. The uncertainty related to the latter is typically large. Up to 20% difference in the estimated long-term emission value were reported in literature depending on which approach was used to determine gas concentrations in the incoming and outgoing air (Janke et al., 2020). In our dataset, the difference in the average emission values was even 21% or 27% (depending on which emission value was used as the baseline value). In general, we observed a smaller deviation between the simulated and the experimentally derived emission when using the CO_2 balancing approach based on the average indoor concentration. At the same time, the largest individual deviations between simulations and experimentally derived emissions were found when using this approach. This can be explained by the fact that the averaging approach is known to be particularly robust under fluctuating wind conditions, but it also tends to underestimate the gas concentration in the outgoing air (Janke et al., 2020). As can be seen in Fig. 8 the largest deviations between model and measurement based emission time series were observed in situation where the measured concentration differences were very low, which is more likely in the situation when using the average indoor concentration. In those cases, however, the experimentally derived emission values are also particularly uncertain.

We noticed that the simulated emission time series correlated much better with the emission time series derived from the average indoor concentration than the time series of the two balancing approaches compared to each other. This indicates that the major emission relevant processes were well represented in the model. As shown in Fig. 7 the relative deviation between simulation and measurement was in most settings comparable to the typically reported uncertainty for projections based on intermittent emission measurement (Hempel et al., 2020). However, the time series shown in Fig. 6 also clearly indicates intermittent periods of anti-correlation between the model and the measurements. Similar pattern of deviation on the hourly basis were also reported in the study of Monteny (2015) who simulated NH_3 emissions

Table 3
Correlations between the CO_2 balance based emission estimation using averaged indoor gas concentrations and different simulation options. The full model includes the alkalizing of the slurry as a consequence of the emission processes, the cooling of the urine puddles from body to ambient temperature in the course of time, the downscaling of the wind speed from inflow reference to group specific near-surface wind speed and excretion behavior documented in literature for grazing cattle. In the case of the pH sensitivity study, we compared the option "dependent" (i.e., from the full model) with the options "asymptotic" (i.e., the pH is set to the maximal value already in the first integration step), "average" (i.e., the pH is fixed at the average value between initial and maximal value) and "initial" (i.e., the pH is fixed at the initial value). In the T sensitivity study, we compared the option "cooling" (i.e., from the full model) with the options "ambient" (i.e., slurry temperature is set to ambient temperature already in the first integration step), "daymean" (i.e., slurry temperature is set equal to the ambient daily mean temperature associate with the excretion event) and "average" (i.e., slurry temperature is fixed at the average value between body and ambient air temperature). In the WS sensitivity study, we compared the option "CFDgroups" (i.e., from the full model) with the options "CFDaverage" (i.e., one scaling factor averaged over the four groups), "logprofile" (i.e., downscaling assuming on a logarithmic wind profile) and "inflow" (i.e., no downscaling). Finally in the Urine sensitivity study, we compared the option "grazing" (i.e., from the full model) with the options "exponential" (i.e., an exponential decay of urination volume from morning to night), "uniform" (i.e., an uniform distribution of the total urine volume over the day) and "triggered" (i.e., an almost uniform distribution of the total urine volume over the day where hours with feeding or milking activity were double-weighted).

options	**c**	**c**
simulated	**0.41**	**0.42**
full model run	0.61	0.61
pH sensitivity "asymptotic"	0.24	0.21
pH sensitivity "average"	0.62	0.62
pH sensitivity "initial"	0.62	0.62
T sensitivity "ambient"	0.62	0.61
T sensitivity "daymean"	0.62	0.62
T sensitivity "average"	−0.65	−0.65
WS sensitivity "CFDaverage"	0.52	0.52
WS sensitivity "logprofile"	0.53	0.53
WS sensitivity "inflow"	0.51	0.51
Urine sensitivity "exponential"	0.62	0.62
Urine sensitivity "uniform"	0.64	0.64
Urine sensitivity "triggered"	0.64	0.64

over two times four days for a slatted floor housing system (Monteny et al., 1998). This might be related to a spatial and temporal variability in the input variables that was not mimicked in the measured and modeled input data.

Furthermore, it was highlighted in Section 3 that the projected emission dynamics showed much less fluctuations than the measurements. This result was likely caused by adopting less fluctuating inputs. For example, urination events and urea contents were modeled as averages over all cows within a group, while preceding experiments showed a large variability of the urea concentration in urine puddles in the barn under consideration with a range between 13 and 277 mol per m^3. The inputs used in our model did not reflect the variability among cows, but only among the four performance groups in the barn. In our simulations, we used simulated total excreted nitrogen in urine as a proxy for the urea excretion, since about 70% to 75% of nitrogen excreted in urine of cattle is typically urea (Spek et al., 2013). In practice this will, however, strongly depend on the diet and the N utilization by the individual cows for milk protein synthesis. The fraction between urea and non-urea nitrogen is not constant and ranges between 60% to 90%. Moreover, the ratio will change with the age of the urine puddle due to the activity of urease. In addition, also the urine nitrogen concentration itself is varying largely among cows of the same herd and even between individual urination events (Misselbrook et al., 2016). All of this variation is not captured in the present model. Moreover, when modelling the emissions per group of animals we assumed spatially averaged meteorological conditions, while earlier studies as well as the above-mentioned preceding experiments indicate significant spatial variability (Hempel et al., 2018; Doumbia et al., 2021). The comparison of our simulation runs with group-wise downscaling of the wind speed versus barn average downscaling of the wind speed confirmed the relevance of this spatial variability of meteorological boundary conditions. Finally, in our model we assumed that fluctuations in the boundary conditions within one hour are neglectable. In consequence, the boundary conditions in the model were updated only on an hourly time scale, whereas the actual meteorological conditions may fluctuate much more on a shorter time scale.

In consequence, our model is expected to provide a spatially averaged and temporally smoothed emission pattern. The predictions were consistent with the above-described systematic deviations on the shorter time scale and the pronounced long-term emission pattern fits well with the experimentally derived emission patterns.

4.2. *Uncertainty and sensitivity related to submodules*

Each of the submodules used in this study modeled the state of the input for the reaction kinetics model associated with a particular level of uncertainty which propagated into uncertainty of the predicted emissions.

The pH model, which we used in our study to describe the alkalizing of the slurry puddle over time, was based on an empirical relation reported by Snoek (2016) (Snoek et al., 2016). In the study these authors found a good overall performance of the empirical model reflected in high coefficients of determination per puddle (R^2=0.97±0.04 and ranging from $R^2 = 0.84$ to $R^2 > 0.99$). But they also reported a high variability in the estimated coefficients per individual puddle. Due to the limited number of available measurements in our study we assumed that the ratio of the factors related to NH_3 and CO_2 emissions in our model is equal to the average ratio in the mentioned literature and the asymptotic pH can be described by the regression equation from that publication, while we fitted the two alkalizing rates to the sample measurements in the present study. This was a strong simplification, whereas our sensitivity study indicated that the temporal changes in the alkalizing rates, are particularly relevant to reproduce the long-term emission pattern correctly. For example, even when the pH value was initially set to the asymptotic pH value, the high emission values in summer could not be reproduced. Moreover, this resulted in a strong decrease of the correlation, while the other tested pH input options affected the correlation only marginally. This indicated that pH is particularly important to simulate the first phase of the emission correctly. In consequence, we conclude that the correct determination of the initial pH value and the alkalizing rates are factors of utmost importance in the NH_3 emission modeling. The rates, however, are likely also affected by the actual boundary conditions (i.e., the material of the floor, the ambient temperature, the near-surface wind speed or the relative humidity of the ambient air). For example, Hafner (2013) showed that, when NH_3 and CO_2 are simultaneously emitted, CO_2 emission increases the NH_3 emission rates from thin layers due to an increase in the pH at the manure surface, where the magnitude of the effect depends among others on the manure composition, the temperature and the surface mass transfer coefficient (Hafner et al., 2013). This indicates that a further expansion of the pH submodule, to capture the interaction between the CO_2 and the NH_3 emissions in the course of the alkalizing process of urine, slurry puddles or liquid manure storage, would be valuable for the overall model prediction. Nevertheless, a sufficient description of the pH dynamics on a particular flooring system could likely be estimated as well with measurement efforts, which are much less than efforts needed for representative concentration measurements in naturally ventilated barns.

Reliable predictions of N excreted are needed for an integral assessment of the impact of feeding strategies on the losses of N in dairy cattle farms. Moreover, having overall estimates on urinary N and faecal N is important to calculate the ammoniacal availability, and predict the

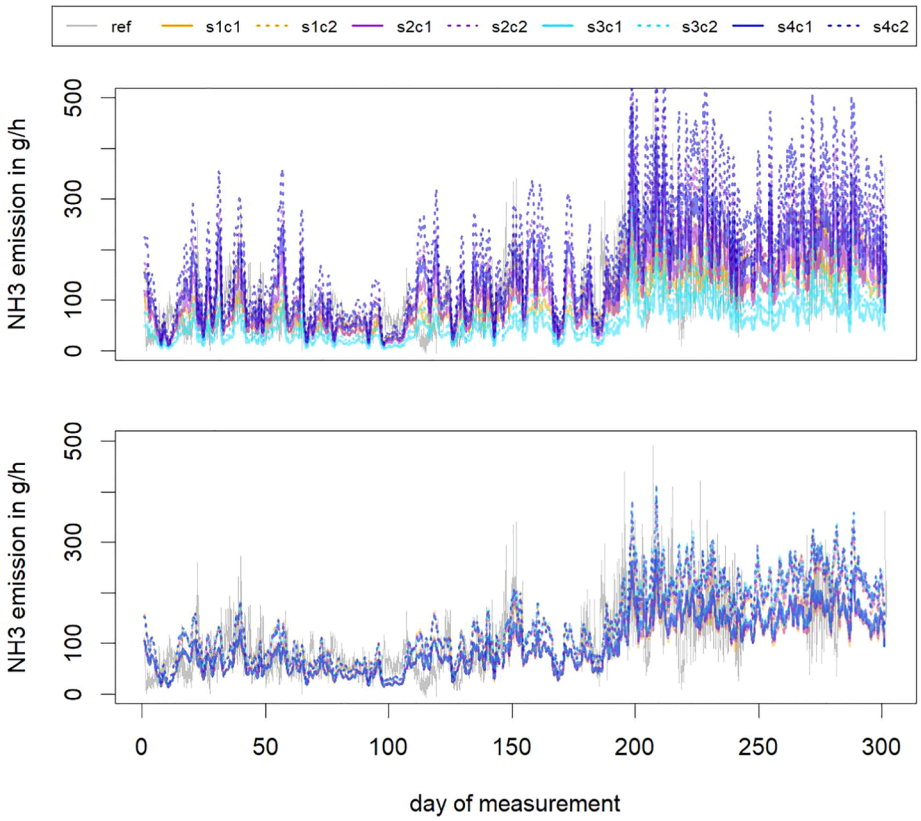

Fig. 11. Sensitivity of the simulated emission dynamics to different wind and urination models models. Comparison between the CO_2 balance based emission estimation using averaged indoor gas concentrations (denoted "ref") and different simulation options where $c1 = 0.41$ and $c2 = 0.42$ refer to the assumed value of scrapping efficiency. The full model includes the alkalizing of the slurry as a consequence of the emission processes, the cooling of the urine puddles from body to ambient temperature in the course of time, the downscaling of the wind speed from inflow reference to group specific near-surface wind speed and excretion behavior documented in literature for grazing cattle. In the WS sensitivity study in the upper panel, we compared the option "s1:CFDgroups" (i.e., from the full model) with the options "s2:CFDaverage" (i.e., one scaling factor averaged over the four groups), "s3:logprofile" (i.e., downscaling assuming on a logarithmic wind profile) and "s4:inflow" (i.e., no downscaling). In the Urine sensitivity study in the lower panel, we compared the option "s1:grazing" (i.e., from the full model) with the options "s2: exponential" (i.e., an exponential decay of urination volume from morning to night), "s3:uniform" (i.e., an uniform distribution of the total urine volume over the day) and "s4:triggered" (i.e., an almost uniform distribution of the total urine volume over the day where hours with feeding or milking activity were double-weighted).

lost in the form of NH_3 and nitrogenous greenhouse gases. This can be approximated by a simple empirical equation, but more mechanistic or process-oriented models simulate with higher accuracy the variation in N excreta depending on input parameters, such as feed quality, N intake and digestibility. Sufficient activity data should be obtainable to generate model inputs, however. For this, the dynamic mechanistic model that was used delivered outputs on total N which was partitioned between N in milk, and N in urine and faces. The model captured the variation between individual groups of cows within which cows have basically the same level of production and feed intake, by calculating an average diet for each category. Assuming that the differences between animals in the same group are not relevant was again a simplification, as in practice these differences may occur (e.g., in feed conversion ratio and in N digestibility) and impact the amount of N excreted in urine and feces. In this sense, using a multivariate Bayesian model Reed (2014) showed that the efficiency with which feed N is converted to milk N, was improved when diet metabolizable energy content was increased, and thus N losses were reduced, improving dairy production efficiency (Reed et al., 2014). In fact, adding metabolizable energy content, as a covariate with N intake improved the predictions of N excretion (Kebreab et al., 2010).

The empirical model used to predict urine volume was driven by DMI, level of milk production and observed or assumed fractions of minerals in dietary DM. This resulted in capturing differences in the amount of urine produced between different groups of animals. However, it should be pointed out that this model applies in particular to conditions where drinking water is not restricted, and relatively high amounts of K and Na are ingested in DMI. Furthermore, timing/ distribution of urination volume over the day had considerable influence on the predicted emission dynamics. Our modeling based on observations published for grazing cattle was insufficient since conditions in the barn (feeding, milking) seems to modify the urination behavior considerably. Moreover, the published distribution of urine volumes per event and in the course of the day were measured under comparably warm conditions in the late summer/ early autumn where activity patterns might be shifted towards night or early morning which could have an effect also on the temporal urination pattern. Further studies relating the urination behavior of housed dairy cattle to activity patterns and ambient conditions could be beneficial to further refine our barn scale NH_3 emission model.

A further submodule, the cooling model, could in principle be refined by taking into account effects of radiation, convective heat transfer and fluctuating ambient air temperatures in general. This would result in a nonlinear response of the temperature that is not captured by the simplified assumptions in the Newton's law of cooling adopted in the present study. However, the submodule had in general a rather small impact on the overall model accuracy in our sensitivity study as long as the cooling dynamics were roughly captured. This indicates that the determination of a sufficiently accurate cooling rate is more important than the determination of the actual ambient air conditions and their fluctuations. Also some influence of thermoconductivity of the floor on cooling rate must be expected, which may contribute to an explanation of emission differences for different floor materials and environmental conditions. As illustrated in literature, the urine temperature (or slurry temperature) drops fast and may end up even in negative differences between the ambient air temperature and the slurry temperature as air temperature is usually not measured directly at the floor (Snoek et al., 2016). Further measurements are needed to investigate the relation between air temperature, floor temperature and slurry temperature for different floor types and materials in detail. The air temperature close to the emission active surface might be simulated using the computational fluid dynamics model, as our sensitivity analysis already showed the potential of including this submodule with regard to local near-surface wind speeds. Incorporating the wind speed variability throughout the barn by using approximated group-wise averaged near-surface wind speeds, already significantly improved the performance of our barn scale NH_3 emission projections. In consequence, more barn-specific numerical simulations taking into account further combinations of boundary

conditions can be expected to further improve the NH_3 emission predictions. In this sense, an online coupling of the NH_3 release and the flow model is desirable.

The main unsolved issue with our barn scale model is, however, its sensitivity on the effective emission active surface area. This is a rather crucial and sensitive model parameter strongly affecting the average amount of NH_3 emission predicted by the model. So far its value has been determined only recursively. In consequence, in the current setting measurement efforts for a suitable estimation might be comparable to the efforts for concentration measurements. Hence, additional measurement setups (preferable at lab scale) are needed to derive the effective area reduction of a floor system/ material in sample measurements. Moreover, on-farm chamber measurements might be an option to collect further crucial insights on the effective cleaning efficiency.

5. Conclusions

Our study demonstrated the great potential of coupling different mechanistic modelling approaches to project NH_3 emission dynamics from dairy housing at the barn scale using only input data that can be easily accessed and measured or monitored cost-efficiently. Our modular model was in general capable to reproduce the long-term emission patterns. The deviations between the modelled and the measured long-term average emission value were in the same order of magnitude as the deviation between the emission values obtained by the different approaches of CO_2 balancing. Uncertainty of model predictions was comparable to the typical uncertainty of projections obtained from regressions based on intermittent measurements. The latter requires more elaborate measurement setups, however, in contrast to modeling with a selected set of inputs. In contrast to the well reproduced long-term dynamics, the predicted short-term emission dynamics showed discrepancies, which is likely related to spatial and temporal averaging of the input data. Further model refinement and/ or adding specific modules that mimic the spatial and temporal variability of those input data can be expected to further improve the overall model performance on the shorter time scales. Sensitivity analysis indicated that this needs to include particularly improved modeling of urination and wind speeds as well as the variability of the urea content and the temporal dynamics of the alkalizing in interaction with the emission of NH_3 and CO_2. Finally, we concluded that the cleaning efficiency of the floor scraping is a crucial and sensitive, but yet insufficiently experimentally determined model parameter.

In consequence, we identified four crucial areas for future research.

First, a detailed investigation of pH dynamics in urine and shallow slurry puddles is urgently needed. On the one hand, this involves the development of a standardized and refined procedure for the estimation of the initial pH value in the puddle, as the results of the two approaches described in this paper (i.e., sample measurements or the calculation from the dietary cation–anion difference) were found to be ambiguous. On the other hand, the empirically derived regression coefficients to describe the pH change over time due to the emission of NH_3 and carbon dioxide are rather sensitive to the available dataset (as was already mentioned in literature before). Therefore, future work should focus on (partly) replacing those empirical relations also by a mechanistic pH model, which should also take into account potential interactions with the floor material.

Second, a detailed investigation of the distribution of the urination volume among the individual cattle and in the course of the day should be performed under practical conditions inside a barn. In order to reach the goal of deriving an emission estimation tool that requires minimal measurement efforts, options to determine the timing and volume of urination noninvasive have to be considered. Attempts in this direction may include the application of machine learning approaches on camera and radar data.

Third, in order to improve the representation of the scrapping procedure in the barn scale model, the influence of different factors (e.g., floor material and microclimatic conditions) on the actual scrapping efficiency has to be investigated in detail. In this context, measurements with static and/or dynamic flux hoods might provide new insights.

Finally, the feasibility of an active coupling of the volatilization model with the air flow model (instead of the one-way-coupling in the presented approach) has to be investigated. In this context, research should also include the investigation of approaches to approximate spatially resolved near-surface air flow by means of machine learning in order to keep the overall computing times reasonable for practical applications.

Declaration of Competing Interest

The authors declare that they have no known competing financial interests or personal relationships that could have appeared to influence the work reported in this paper.

Appendix A. Acknowledgement

We thank Ulrich Stollberg, Andreas Reinhardt, Senthilathiban Swaminathan and Ida Anheier for assistance in the data collection. We further acknowledge fruitful discussions with André Aarnink and Nico Ogink on the implementation of the model core.

Appendix B. Funding

This research did not receive any specific grant from funding agencies in the public, commercial, or not-for-profit sectors.

Appendix C. Author contributions

Sabrina Hempel: Conceptualization, Methodology, Software Validation, Formal analysis, Original Draft, Review & Editing, Visualization; Latifa Ouatahar: Methodology, Software, Validation, Formal Analysis, Data Curation, Review & Editing; David Janke: Conceptualization, Validation, Formal Analysis, Investigation, Resources, Data Curation, Review & Editing; Moustapha Doumbia: Methodology, Software, Validation, Review & Editing; Dilya Willink: Conceptualization, Methodology, Software, Validation, Investigation, Resources, Review & Editing, Visualization; Barbara Amon: Conceptualization, Validation, Review & Editing, Supervision; Andre Bannink: Methodology, Software, Validation, Review & Editing, Supervision; Thomas Amon: Conceptualization, Validation, Resources, Review & Editing, Supervision.

References

Aland, A., Lidfors, L., Ekesbo, I., 2002. Diurnal distribution of dairy cow defecation and urination. Appl. Anim. Behav. Sci. 78 (1), 43–54.

Amon, B., Cinar, G., Anderl, M., Dragoni, F., Pierer, M.K., Hörtenhuber, S., 2021. Inventory reporting of livestock emissions: the impact of the ipcc 1996 and 2006 guidelines. Environ. Res. Lett.

Bannink, A., van Vuuren, A.M., 1998. Kation-anionverschil in melkvee-rantsoenen als methode om urine ph en ammoniakemissie te beinvloeden [cation anion difference in dairy cow rations as a measure to influence urine ph and ammonia emission], in: ID-DLO rapport No. 98.032, 1998.

Bannink, A., Valk, H., Van Vuuren, A., 1999. Intake and excretion of sodium, potassium, and nitrogen and the effects on urine production by lactating dairy cows. J. Dairy Sci. 82 (5), 1008–1018.

Bannink, A., Spek, W.J., Dijkstra, J., Šebek, L.B., 2018. A tier 3 method for enteric methane in dairy cows applied for fecal n digestibility in the ammonia inventory. Front. Sustain. Food Syst., 2018, 66.

Betteridge, K., Costall, D., Li, F., Luo, D., Ganesh, S., 2013. Why we need to know what and where cows are urinating-a urine sensor to improve nitrogen models. In: Proceedings of the New Zealand Grassland Association, pp. 119–124.

Cheng, L., Ye, Z., Cheng, S., Guo, X., 2021. Agricultural ammonia emissions and its impact on pm2. 5 concentrations in the beijing–tianjin–hebei region from 2000 to 2018. Environ. Pollut. 291, 118162.

de Vries, W., 2021. Impacts of nitrogen emissions on ecosystems and human health: A mini review. Curr. Opin. Environ. Sci. Health 100249.

Dijkstra, J., Neal, H.D.S.C., Beever, D.E., France, J., 1992. Simulation of nutrient digestion, absorption, and outflow in the rumen: model description. J. Nutr. 122, 2239–2256. https://doi.org/10.1093/jn/122.11.2239.

Dijkstra, J., Bannink, A., Bosma, P.M., Lantinga, E.A., Reijs, J.W., 2018. Modeling the effect of nutritional strategies for dairy cows on the composition of excreta nitrogen. Front. Sustain. Food Syst. 2 (63), 1–16.

Doumbia, E.M., Janke, D., Yi, Q., Zhang, G., Amon, T., Kriegel, M., Hempel, S., 2021. On finding the right sampling line height through a parametric study of gas dispersion in a nvb. Appl. Sci. 11 (10), 4560.

Doumbia, E.M., Janke, D., Yi, Q., Amon, T., Kriegel, M., Hempel, S., 2021. Cfd modelling of an animal occupied zone using an anisotropic porous medium model with velocity depended resistance parameters. Comput. Electron. Agric. 181, 105950.

D'Urso, P.R., Arcidiacono, C., Valenti, F., Cascone, G., 2021. Assessing influence factors on daily ammonia and greenhouse gas concentrations from an open-sided cubicle barn in hot mediterranean climate. Animals 11 (5), 1400.

Elzing, A., Monteny, G., 1997. Modeling and experimental determination of ammonia emissions rates from a scale model dairy-cow house. Trans. ASAE 40 (3), 721–726.

Hafner, S.D., Montes, F., Rotz, C.A., 2013. The role of carbon dioxide in emission of ammonia from manure. Atmos. Environ. 66, 63–71.

Hempel, S., König, M., Menz, C., Janke, D., Amon, B., Banhazi, T.M., Estellés, F., Amon, T., 2018. Uncertainty in the measurement of indoor temperature and humidity in naturally ventilated dairy buildings as influenced by measurement technique and data variability. Biosyst. Eng. 166, 58–75.

Hempel, S., Adolphs, J., Landwehr, N., Janke, D., Amon, T., 2020. How the selection of training data and modeling approach affects the estimation of ammonia emissions from a naturally ventilated dairy barn–classical statistics versus machine learning. Sustainability 12 (3), 1030.

International VERA Secretariat, Vera test protocol for livestock housing and management systems - version 2018–09, 3rd edition, https://www.vera-verification.eu/app/uploads/sites/9/2019/05/VERA_Testprotocol_Housing_v3_2018.pdf, last access: 01-11-2021.

Janke, D., Willink, D., Ammon, C., Hempel, S., Schrade, S., Demeyer, P., Hartung, E., Amon, B., Ogink, N., Amon, T., 2020. Calculation of ventilation rates and ammonia emissions: Comparison of sampling strategies for a naturally ventilated dairy barn. Biosyst. Eng. 198, 15–30.

Kebreab, E., Strathe, A., Dijkstra, J., Mills, J.A., Reynolds, C.K., Crompton, L.A. Yan, T., France, J., et al., 2010. Energy and protein interactions and their effect on nitrogen excretion in dairy cows. In: Symp. on Energy and Protein Metabolism and Nutrition, Parma, Italy, 2010, pp. 417–426.

Lal, R., 2021. Climate change and agriculture. In: Clim. Change. Elsevier, pp. 661–686.

Misselbrook, T., Fleming, H., Camp, V., Umstatter, C., Duthie, C.-A., Nicoll, L., Waterhouse, T., 2016. Automated monitoring of urination events from grazing cattle. Agric., Ecosyst. Environ. 230, 191–198.

Monteny, G., Schulte, D., Elzing, A., Lamaker, E., 1998. A conceptual mechanistic model for the ammonia emissions from free stall cubicle dairy cow houses. Trans. ASAE 41 (1), 193.

Murawska, A., Prus, P., 2021. The progress of sustainable management of ammonia emissions from agriculture in european union states including poland—variation, trends, and economic conditions. Sustainability 13 (3), 1035.

Oenema, O., Bannink, A., Sommer, S.G., Van Groenigen, J., Velthof, G., 2008. Gaseous nitrogen emissions from livestock farming systems. In: Nitrogen in the Environment. Elsevier, pp. 395–441.

Piccione, G., Caola, G., Refinetti, R., 2003. Daily and estrous rhythmicity of body temperature in domestic cattle. BMC Physiol. 3 (1), 1–8.

Reed, K., Moraes, L., Fadel, J., Casper, D.P., Dijkstra, J., France, J., Kebreab, E., 2014. Prediction of nitrogen use in dairy cattle: a multivariate bayesian approach. Anim. Prod. Sci. 54 (12), 1918–1926.

Robichaud, M.V., de Passillé, A., Pellerin, D., Rushen, J., 2011. When and where do dairy cows defecate and urinate? J. Dairy Sci. 94 (10), 4889–4896.

Schmithausen, A.J., Schiefler, I., Trimborn, M., Gerlach, K., Südekum, K.-H., Pries, M., Büscher, W., 2018. Quantification of methane and ammonia emissions in a naturally ventilated barn by using defined criteria to calculate emission rates. Animals 8 (5), 75.

Schrade, S., Zeyer, K., Gygax, L., Emmenegger, L., Hartung, E., Keck, M., 2012. Ammonia emissions and emission factors of naturally ventilated dairy housing with solid floors and an outdoor exercise area in switzerland. Atmos. Environ. 47, 183–194.

Snoek, D.J., Ogink, N.W., Stigter, J.D., Van de Weijer, T.M., Koerkamp, P.W.G., et al., 2016. Dynamic behavior of ph in fresh urine puddles of dairy cows. Trans. ASABE 59 (5), 1403–1411.

Spek, J., Dijkstra, J., van Duinkerken, G., Hendriks, W.H., Bannink, A., 2013. Prediction of urinary nitrogen and urinary urea nitrogen excretion by lactating dairy cattle in northwestern Europe and North America: A meta-analysis. J. Dairy Sci. 96 (7), 4310–4322.

Wang, H., Aguirre-Villegas, H.A., Larson, R.A., Alkan-Ozkaynak, A., 2019. Physical properties of dairy manure pre-and post-anaerobic digestion. Appl. Sci. 9 (13), 2703.

Wu, W., Zhang, G., Kai, P., 2012. Ammonia and methane emissions from two naturally ventilated dairy cattle buildings and the influence of climatic factors on ammonia emissions. Atmos. Environ. 61, 232–243.